

HDX-MS Combining Molecular Dynamics Simulation Reveals Structural Basis of Transcriptional Coactivator PC4 Binding to a Platinum Crosslinked Double-Stranded DNA

Yuanyuan Wang,^{a,b,‡} Zhifeng Du,^{a,c,‡} Lifang Chen,^{d,‡} Yao Zhao,^{*a} Wei Zheng,^a Juan Qiao,^a Kui Wu,^e Hui Zhang,^d Qun Luo,^{a,b} Li Qi,^{a,b} Xin Zhang^{*d} and Fuyi Wang^{*a,b,f}

^a Beijing National Laboratory for Molecular Science; CAS Research/Education Centre for Excellence in Molecular Sciences; National Centre for Mass Spectrometry in Beijing, CAS Key Laboratory of Analytical Chemistry for Living Biosystems, Institute of Chemistry, Chinese Academy of Sciences, Beijing 100190, People's Republic of China.

^b University of Chinese Academy of Sciences, Beijing 100049, People's Republic of China.

^c School of pharmacy, Huazhong University of Science and Technology, Wuhan, Hubei, 430030, People's Republic of China.

^d State Key Laboratory of Chemical Resource Engineering, Beijing Advanced Innovation Center for Soft Matter Science and Engineering, Beijing University of Chemical Technology, Beijing 100029, People's Republic of China.

^e Key Laboratory of Hubei Province for Coal Conversion and New Carbon Materials; School of Chemistry and Chemical Engineering, Wuhan University of Science and Technology, Wuhan, 430081, People's Republic of China.

^f Shandong University of Traditional Chinese Medicine, Jinan 250355, People's Republic of China.

[‡] These authors contributed equally to this work.

* To whom correspondence should be addressed. Emails: yaozhao@iccas.ac.cn; fuyi.wang@iccas.ac.cn; zhangxin@mail.buct.edu.cn

ABSTRACT: Human nuclear protein positive cofactor PC4 is a DNA-binding protein, and plays an important role in the early response to DNA damage by recognizing single-stranded oligodeoxynucleotide domain and facilitating the subsequent steps of DNA repair. Our group previously discovered that PC4 selectively binds to a double-stranded oligodeoxynucleotide (dsODN) damaged by a *trans*-platinum anticancer complex, *trans*-[PtCl₂(NH₃)(thiazole)] (*trans*-PtTz). However, the molecular basis of this unique recognition and interaction remained unclear. In this work, amide hydrogen/deuterium exchange mass spectrometry (HDX-MS) was applied to dissect the interaction interface between PC4 and a 15-mer double-stranded oligodeoxynucleotide crosslinked by *trans*-PtTz (*trans*-PtTz-dsODN). Global deuterium uptake suggested a 1:1 binding stoichiometry of PC4 to *trans*-PtTz-dsODN. Local deuterium uptake revealed that the flexible N-terminal loop and the β3 – β5-sheet played key roles in the recognition and interaction between PC4 and *trans*-PtTz-dsODN. In order to locate the key amino acid residues, molecular dynamics simulation was employed, demonstrating that PC4 binds to the *trans*-PtTz-dsODN at the minor groove *via* strong H-bonds with the nucleobases of the complementary strand. The minor groove width was broadened to adapt for the binding of PC4. Arg86 residue in PC4 was shown to dominate the recognition and interaction, which was verified by

electrophoretic mobility shift assays. This work profiles the detailed interaction mechanism of PC4 with *trans*-PtTz damaged dsODN, and the combination use of HDX-MS and molecular dynamics simulation provides a new paradigm for the future research of the cellular response to the platinum induced DNA damage.

Introduction

Human nuclear protein positive cofactor 4 (PC4) is an abundant multifunctional nuclear protein that play important roles in various cellular processes such as transcription, DNA repair, replication, chromatin organization and cell cycle progression.¹⁻⁵ Usually, PC4 tends to form a homodimer, giving two DNA binding interfaces, so as to accommodate single-stranded DNA (ssDNA)⁶⁻⁸ at DNA damage sites and recruit various proteins to exert their corresponding functions. PC4 might halt transcription by recognizing and stabilizing unpaired double-stranded DNA (dsDNA), ssDNA and DNA ends.⁹⁻¹⁰ The common DNA repair intermediates or structures generated at DNA damage sites may also be recognized by PC4 to enable detection and repair of these lesions by introducing other DNA damage repair factors.^{6, 11-12} PC4 has also been reported to activate double-strand break repair by stimulating the joining of non-complementary DNA ends.¹³ These indicate that PC4 plays an important role in the early response to DNA damage by recognizing ssDNA.¹⁴

DNA encodes genetic information and has long been considered as a preferential target for cancer chemotherapeutic agents.¹⁰ The coordination of the widely used anticancer drug, cisplatin, to purine bases mainly forms 1,2-intrastrand crosslinks to distort DNA conformation by unwinding and bending the helix.¹⁵ Such unique and severe lesions in DNA will halt the normal transcription and can be specially recognized by high mobility group (HMG) domain proteins, particularly HMGB1, which in turn impedes the repair of damaged sites and leads to apoptosis of cancer cells.¹⁶

On the contrary, as the inactive stereoisomer of cisplatin, transplatin (*trans*-diamminedichloroplatinum), mainly forms monofunctional and 1,3-GXG intrastrand crosslinking adducts and less interstrand crosslinked DNA adducts.¹⁷ The interactions of cellular proteins with *trans*-platinum complex damaged DNA is still an open question. *Trans*-PtTz (*trans*-[PtCl₂(NH₃)(thiazole)]) shares the same geometry as transplatin but has significantly enhanced cytotoxicity, even to cisplatin-resistant cancer cell lines.¹⁸ *Trans*-PtTz was shown to form monofunctional, 1,3-GXG intrastrand crosslinked and 1,2-GG interstrand crosslinked DNA adducts nearly in equal amount, and it was believed that the overall drug cytotoxicity of *trans*-PtTz could be the sum of the contributions of each of these adducts.¹⁹ Therefore, it is important to investigate the roles of DNA adducts formed by *trans*-PtTz, especially the recognition and interactions of these different adducts with cellular proteins, which is significant for better understanding of the mechanisms of action of various *trans*-platinum complexes.

Our group has previously developed a strategy combining affinity DNA probe and MS-based proteomics, enabling us to discover that PC4 selectively binds to 1,3-GTG intrastrand crosslinked DNA by *trans*-PtTz.²⁰ Although PC4 has been reported to be a cofactor to bind to ssDNA at the damage sites,^{14, 21} this was the first time to report that PC4 preferentially binds to this special type of double-stranded DNA containing platinum induced damage. However, the structural basis of this unique recognition and interaction is still not clear and intrigued us to investigate urgently.

Hydrogen/deuterium exchange coupled with mass spectrometry (HDX-MS) has emerged as a rapid and sensitive approach for characterization of perturbations in conformational change of proteins following ligand binding.²²⁻²³ The exchange rates between backbone amide hydrogens and deuterium of D₂O can be examined by MS so as to monitor the changes of the local environment, and the structural

and dynamic aspects of proteins in solution.²⁴ The binding interfaces to the peptide level upon the formation of protein-ligands complex can be revealed by detecting changes in local deuterium uptake from digestion of deuterated proteins.²⁵⁻²⁶ By comparing the difference of exchanged H/D number between the proteins in different state, the interaction information with various molecules on the protein surface can be obtained.²⁷ Unlike X-ray crystallography requiring crystallization process of protein-DNA complexes and NMR needing large amount of purified samples, mass spectrometry has high resolution and sensitivity, so only a small amount of sample in solution (< 1 mg/experiment at low mM concentration) is enough to obtain useful information, even for large proteins and ligands.²⁸

In this work, the recognition and interaction of a 1,3-intrastrand crosslinked 15-mer double strand oligodeoxynucleotide (dsODN), in which *trans*-PtTz binds to a -GTG- moiety, with the human nuclear protein positive cofactor PC4 is investigated using HDX-MS coupled to an homemade online pepsin digestion device. Molecular dynamics simulation was also employed to interpret the experimentally determined interaction and produced a molecular model to unravel more conformation details of the PC4-*trans*-PtTz-dsODN ternary complex. Electrophoretic mobility shift assay (EMSA) was carried out to further verify the key binding amino acid residues at the protein-ODN interface.

Experimental

Materials and methods

Starting materials *trans*-[PtCl₂(NH₃)(thiazole)] (*trans*-PtTz; Figure 1) was prepared following the procedure reported previously.²⁹ The PC4 protein was obtained from Proteintech (Wuhan, China). The sequence of human PC4 protein were adopted from Uniprot database align No.: P53999. Pepsinogen was purchased from Sigma-Aldrich and used without further purification. Deuterium oxide (99.9%), formic acid (FA) and protamine sulfate were all purchased from Sigma. The complementary single-stranded oligodeoxynucleotides (ODNs) **I** (5'-CTCTTGTTCTTCT-3') and **II** (5'-AGAAGAACAAGAG-3') were obtained from TaKaRa (Dalian, China; Figure 1). The solvents (water and acetonitrile) for mobile phases used in MS and HPLC were all purchased from Fisher. Other aqueous solutions were prepared using MilliQ water (Milli-Q Reagent Water System).

Preparation of platinated dsODN The 1,3-GTG intrastrand crosslinked single-stranded ODN **I** by *trans*-PtTz and the dsODN containing the *trans*-PtTz damage site was prepared following the procedure described in the our previous report.²⁰ Briefly, *trans*-PtTz was incubated with the -GTG-containing single-stranded **I** at a molar ratio of 0.8:1 at 37 °C for 3 days. Then the 1,3-GTG intrastrand crosslinked strand **I** was purified by HPLC with a C8 column (4.6 × 250 mm, 5 μm, Agilent) on an Agilent 1200 HPLC system where the mobile phases were water containing 20 mM TEAA and acetonitrile containing 20 mM TEAA. The purified *trans*-PtTz 1,3-GTG intrastrand crosslinked ODN **I** was characterized by ESI-MS and quantified by UV-visible spectrometer and then lyophilized. Thereafter, the platinated ODN **I** mixed with equal mole of the complementary strand **II** in 100 mM NaClO₄ was heated to 85 °C, sustained for 5 min and cooled slowly to room temperature. The formed *trans*-PtTz 1,3-GTG intrastrand crosslinked double-stranded ODN **III** (1,3-*trans*-PtTz-**III**) was stored at -20 °C before use.

H/D exchange protocol PC4 protein solutions (100 μM) were prepared in 20 mM HEPES (pH 7.4) containing 100 mM NaCl. Titration experiments started with the equilibration of PC4 (100 μM) with varying concentrations of 1,3-*trans*-PtTz-**III** in more than 2 h.

For global deuterium uptake, the apo-PC4 (free intact protein) was incubated with 2 equiv. mol of 1,3-*trans*-PtTz-**III** in buffer (pH 7.4) containing 20 mM HEPES and 200 mM NaCl (pH 7.4) at 295 K for 120 min to give holo-PC4 (1,3-*trans*-PtTz-**III**-PC4). Aliquot (9 μ L) of D₂O was added to 1 μ L of apo-PC4 and holo-PC4, respectively, to initiate H/D exchange, where the concentration of was D₂O 90%. After various incubation time, the HDX was quenched with 1 μ L ice-cold FA (20%) (holo-PC4 sample also containing 10:1 mol equiv. of protamine sulfate and 1,3-*trans*-PtTz-**III**) to give a final pH of 2.5. Protamine sulfate was used to remove excess of platinated ODN from the ODN-PC4 complexes prior to MS analysis. Deuterated protein was loaded immediately on an Inertsil WP300 C8 column (2.1 \times 50 mm, 5 μ m, GL Sciences) and separated with use of mobile phase A (0.1% FA in water) and B (0.1% FA in acetonitrile). A gradient from 10% – 60% B within 6 min at 2 \pm 0.2 $^{\circ}$ C was used to elute the proteins directly into the mass spectrometer for analysis.

To determine the local deuterium uptake, an online pepsin digestion column applied in the HPLC system coupled with ESI-MS was developed, as shown in Scheme 1. The online pepsin digestion column was fabricated by immobilizing the pepsinogen on sub-micron skeletal polymer monolith as previously reported.³⁰ The residual epoxide groups were blocked by 1 mg mL⁻¹ aspartic acid in 50 mM Tris-HCl buffer (pH 7.5) for 1 h. The immobilized pepsinogen column was activated by 10 column volumes of 0.1% FA (pH 2.5) passing through the column prior to incubating with 2 mg mL⁻¹ soluble porcine pepsin for 16 h at 37 $^{\circ}$ C.³¹ Then the activated pepsinogen column was rinsed with 50 column volumes of 0.1% FA (pH 2.5) to remove non-immobilized pepsin prior to use. The mixture of PC4 and platinated ODN **III** in 90% D₂O was quenched with 20% FA after deuterium exchange for requested times and then injected into the system using valve A (Rheodyne valve Model 7725i) equipped with a 10- μ L loop maintained a 2 \pm 0.2 $^{\circ}$ C (Scheme 1). This injector was connected to a column (4.6 \times 50 mm) packed with immobilized pepsin. Mobile phase (0.1% FA, pH 2.5, flow rate 210 μ L min⁻¹) from pump C (LC-20AD, Shimadzu) carried the protein from the injection loop to the pepsin column where the protein was digested into peptides at 2 \pm 0.2 $^{\circ}$ C. The same mobile phase carried the peptides to a trap column (C18, 4.6 \times 20 mm; Waters) where the D-labeled peptides were concentrated and desalted. Mobile phases A (0.1% FA/H₂O) and B (0.1% FA/acetonitrile) were applied to separate the peptides from the trap column through valve B (Rheodyne 7000 switching valve, Scheme 1) and the HPLC column (Ultimate AQ-C18, 2.1 \times 50 mm, 5 μ m, Welch) to the ESI-MS probe. A gradient from 15% to 50% of mobile phase B in 6 min was used for peptide separation. When deuterated samples were analyzed, part of the system, including the valves A and B, the sample loop, the pepsin column, the C18 trap column and the analytical column were maintained at 2 \pm 0.2 $^{\circ}$ C in a house-made precise temperature control refrigerator (50 \times 50 \times 50 cm³) (refer to Scheme 1). The global or local deuterium uptake ratio was calculated by using equation 1 as follow,

$$\text{Deuterium\%} = \frac{M_{HDX} - M_{control}}{(N-2) \times 0.9} \times 100\% \quad (1)$$

where M_{HDX} is the centroid mass of a deuterated protein/peptide, $M_{control}$ is the centroid mass of the corresponding non-deuterated protein/peptide, N is the number of amino acids in the protein/peptide, (N – 2) is the number of exchangeable amide hydrogens, and 0.9 presents the final D₂O content of the buffer system.

Electrospray ionization mass spectrometry (ESI-MS) Positive-ion ESI-MS were obtained on a Xevo G2 Q-TOF coupled to a Waters ACQUITY H-class HPLC system (Waters). The solvent tubes and columns were all maintained at 2 ± 0.2 °C to minimize back-exchange of amide hydrogen. The capillary voltage was 3 kV, sample cone 40 V and extraction cone 4 V. The desolvation temperature was 623 K and source temperature 373 K. Nitrogen was used as desolvation gas with a flow rate of 600 L h⁻¹. Global deuterium uptake spectra and local deuterium uptake spectra were acquired in the range of m/z 100 – 2000. All analysis were performed with “lockspray” to ensure accuracy and reproducibility. Leucine–enkephalin was used as the “lockmass” calibration at a concentration of 2 ng μL^{-1} and flow rate of 10 $\mu\text{L min}^{-1}$. MS Data were collected in continuum mode, the lockspray frequency was once every 10 s, and the data were averaged over 10 scans. MassLynx (ver. 4.1), Biopharmalynx (ver. 1.3) and HX-Express (ver. 2)³² were used for data collection, analysis and processing.

Molecular dynamics simulations The 3D structure of M63 – L127 of PC4 was downloaded from the PDB (Code: 2C62)⁷ and the N-terminal loop residues M1 – N62 were manually added to generate 3D structure of full length PC4 by Discovery Studio 3.5. All the molecular dynamics simulations of holo-PC4 complexes were performed using the Sander module of Amber14 package.³³

The optimization of *trans*-PtTz were carried out at $\omega\text{B97X-D/BSI level}^{34}$ by using Gaussian 09 program package.³⁵ LANL2DZ ECP basis sets were applied to Pt metal center, and 6-31G* basis sets were used for C, N, Cl, S, H atoms. The geometric parameters of *trans*-PtTz were generated by VFFDT software.³⁶ The double-stranded ODN **III** was constructed in B form by using Nucleic Acid Builder (NAB) in Amber14 program package.³³ The minor/major groove distance of ODN were analyzed with CURVES+ program.³⁷

For the stimulations of 1,3-*trans*-PtTz-**III**-PC4 (holo-PC4) complex, ff14SB and general Amber force field (GAFF)³⁸ were employed. The ODN-protein complex was solvated by 8 Å TIP3P water molecules with periodic boundary conditions. Cl⁻ or Na⁺ counter ions were placed around the complex using tleap module in Amber14 package to obtain electrostatic neutrality. The non-bonded interactions cutoff was set as 10 Å. To maintain the structure of *trans*-PtTz in ODN **III**, restraints of 10 kcal mol⁻¹ Å⁻² were applied on the *trans*-PtTz unit and the corresponding side chains of guanines of ODN **III**. Minimization is divided into two processes, i.e. 1500 steps of steepest-descent method and 1500 steps of conjugate gradient method. The holo-PC4 complex was heated from 10 K to 300 K gradually, then followed 60 ps equilibration. The SHAKE algorithm was applied to all bonds involving hydrogen atoms. The 20 ns of molecular dynamics simulations were run for holo-PC4 at constant temperature of 300 K and a pressure of 1 bar. The time step for simulation is 2 fs and the trajectory were recorded every 500 steps. Average conformation of holo-PC4 was extracted from 8 – 20 ns of the trajectory. One conformational snapshot which has the minimum RMSD values with average conformation was chosen as representative conformation of holo-PC4 complex. Cpptraj module in Amber 14 package was employed to calculate the hydrogen bond occupancy in the simulation.

Electrophoretic mobility shift assay Fluorescein-labeled single-stranded ODN **II**, designated as F-**II**, was obtained from Sangon Biotech (Shanghai, China). Fluorescein-labeled 1,3-*trans*-PtTz-**III** was produced by annealing the 1,3-*trans*-PtTz platinated **I** with 1 mol equiv. of F-**II**. For EMSA experiments, aliquot (1 μL) of the fluorescent labeled 1,3-*trans*-PtTz-**III** (1 μM) was mixed with various volumes of PC4 protein (45 μM), and the binding buffer (20 mM HEPES, 100 mM NaCl (pH 7.4) and 10 % (w/v) glycerol) was added to make a final volume of 10 μL . The mixtures were incubated at room temperature for 2 h prior to sampling. The protein-ODN complexes were separated in 6% non-denaturing polyacrylamide gels in 1× Tris-borate-EDTA buffer (pH 8.1) run at 50 V at 4 °C for 60 min. After

electrophoresis, the gels were imaged at excitation wavelength 488 nm and recorded at 600 nm with a Typhoon TRIO Variable Mode Imager (GE Health).

Results

Construction of the platinum crosslinked ODN complex

To construct a model dsODN containing 1,3-GTG intrastrand crosslink by *trans*-PtTz, we synthesized an oligodeoxyribonucleotide (ODN) duplex²⁰ which contains a pyrimidine-rich top strand with only two G bases (Figure 1) separated by one T in between. The top strand **I** was modified by *trans*-PtTz so that it contained a single 1,3-GTG intrastrand crosslink. At the given reaction condition with the molar ratio of Pt/**I** = 0.8, the 1,3-GTG intrastrand crosslinked ODN **I** by *trans*-PtTz was the main adduct which was confirmed by the HPLC analysis. Only one new peak besides the free strand **I** was observed (Figure S1A in the Supporting Information). This product fraction was collected and characterized by ESI-MS where the observed (obs.) m/z 1195.4187 (4^-) and m/z 1594.2341 (3^-) were identified as *trans*-PtTz 1,3-GTG intrastrand crosslinked strand **I** as evidenced by the calculated (calc.) m/z 1195.4219 and m/z 1594.2344, respectively (Figure S1B). Then strand **I** with the 1,3-intrastrand crosslink of *trans*-PtTz was subsequently annealed with its complementary strand **II** in 100 mM NaClO₄ solution to give the 1,3-intrastrand *trans*-PtTz crosslinked duplex ODN (1,3-*trans*-PtTz-**III**) for further use.

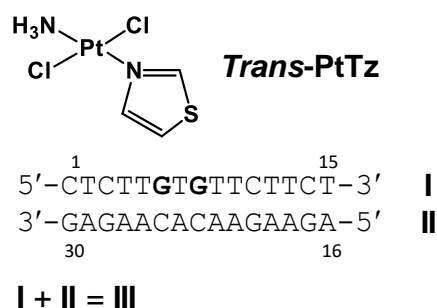


Figure 1. Chemical structure of *trans*-[PtCl₂(NH₃)(thiazole)] (*trans*-PtTz) and the ODN sequences **I**, **II** and double stranded **III** used in this work. The guanines in bold in strand **I** refer to the 1,3-platination sites.

Global H/D exchange

The global amide H/D exchange of PC4 protein with or without ligation with 1,3-*trans*-PtTz-**III** was firstly examined. In order to minimize back-exchange of the amide hydrogens, a fast LC gradient (6 min) was applied to elute the deuterated protein. At low pH (ca. 2.5) required for quenching H/D exchanges of amide hydrogens, all carboxylic groups ($pK_a \approx 4.6$) are protonated, making the proteins positively charged. While on the other hand, the oligodeoxynucleotide still have negative net charges due to the backbone phosphate, which may result in the formation of stable protein/DNA precipitates, and interfere with the HPLC separation and MS analysis of the proteins. Therefore, protamine sulfate was added to avoid co-precipitation of proteins and ODN.³⁹ The global deuterium uptake ratio was calculated by Equation 1 shown in Experimental Section and the corresponding kinetic plots versus time of H/D exchange at 293 K for apo-PC4 (free intact protein) and holo-PC4 (1,3-*trans*-PtTz-**III**-PC4 complex) were obtained by analyzing the corresponding mass spectra (Figure S2), and shown in Figure 2A.

The apo-PC4 approached the maximum deuteration in ca. 20 min of HDX at 293 K (Figure 2A) and an average of 67 backbone amide hydrogens of PC4 were exchanged with deuterium, as indicated by the

maximum mass shift of 67 Da. This number was much less than the 126 total amide hydrogens available for deuterium exchange, and the ratio of deuteration (53.2%) was less than the percent of D₂O used in the experiments (90%). One of the possible reasons is the substantial back exchange of amide hydrogens during HPLC separation. Another possible reasons for the low deuterium ratio of intact PC4 is that some amide hydrogens locating deeply inside the steric conformation of the protein are not solvent accessible. Besides, the formation of homodimer through the contacting of two symmetrical α -helices in opposite direction as revealed by crystallography⁶⁻⁷ may also hamper the deuterium of PC4.

Upon binding with 1,3-*trans*-PtTz-**III**, the number of the deuterium uptake of the PC4 incubated in 90% D₂O for 1 min was only 55, which was substantially less than that of apo-PC4 (Figure 2A). With the increase of incubation time, the number of exchanged deuterium of holo-PC4 quickly increased to 63 in about 10 min, but still lower than that of apo-PC4. These results suggests that the binding of 1,3-*trans*-PtTz-**III** to PC4 significantly shielded the backbone amide hydrogens from exchanging with deuterium in solution. The difference in global deuterium uptake implied the strong and specific binding of PC4 with *trans*-PtTz damaged ODN. The HDX rate as pseudo-first order reactions of the apo-PC4 and holo-PC4 were calculated to be $(4.0 \pm 0.8) \times 10^{-2}$ and $(1.0 \pm 0.1) \times 10^{-3}$, respectively, based on the kinetic curves shown in Figure 2A.

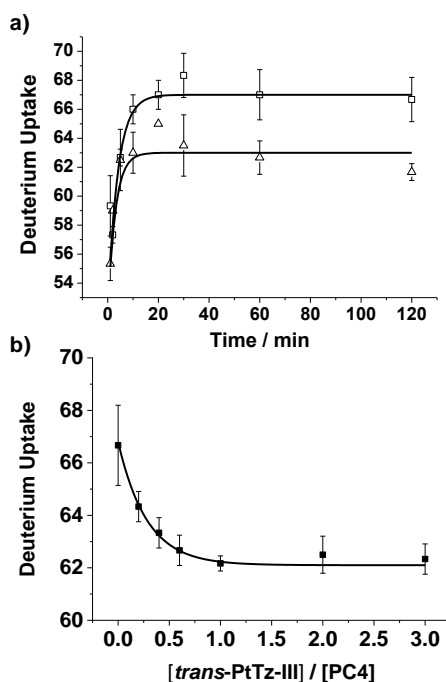


Figure 2. Global deuterium uptake. (a) Kinetic curves for the global deuterium uptake of apo-PC4 (free intact PC4, hollow squares) and holo-PC4 (1,3-*trans*-PtTz-**III**-PC4 complex, hollow triangles). (b) The global deuterium uptake of PC4 versus molar ratio of 1,3-*trans*-PtTz-**III** to PC4. The hydrogen/deuterium exchange time for B was 60 min at 293 K, and the numbers of the deuterium uptake shown in A and B are the means of three independent measurements.

The binding stoichiometry was determined by titrating PC4 (100 μ M) with various concentrations of 1,3-*trans*-PtTz-**III** (from 0 to 300 μ M) at pH 7.4. After quenching the hydrogen/deuterium exchange with 20% FA and back-exchange of the labile hydrogens, the protein was introduced to the HPLC and mass spectrometer to determine the global deuterium uptake under different reaction molar ratios. The global deuterium uptake of the protein was plotted as the function of the molar ratio of 1,3-*trans*-PtTz-

III to PC4 (Figure 2B). With the increased concentration of 1,3-*trans*-PtTz-**III**, the global deuterium uptake of PC4 sharply decreased at the beginning, and then reached an equilibrium when the number of the deuterium uptake of PC4 decreased to 62. The maximum number of deuterium uptake for holo-PC4 in the titration experiment was similar to that for global deuterium uptake. The turning point of the plot indicated that one protein molecule can only bind to one platinated ODN molecule (1,3-*trans*-PtTz-**III**).

Local H/D exchange

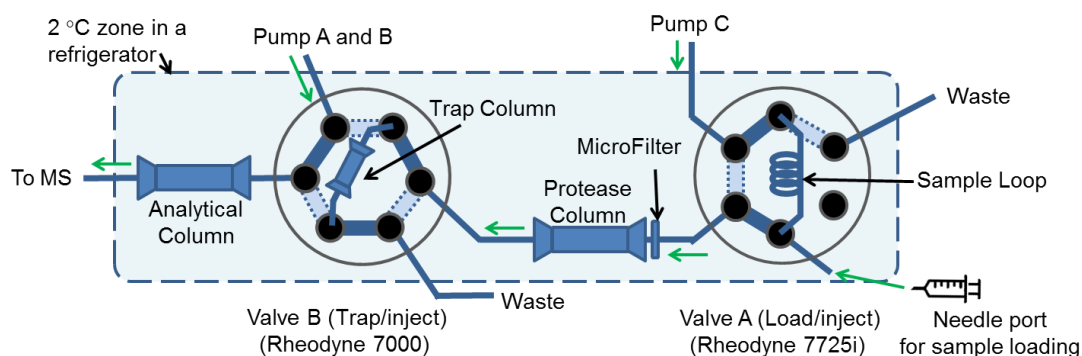
The difference between the global HDX reactions of apo-PC4 and holo-PC4 drove us to explore further the details of the difference by local HDX experiments. To efficiently and accurately determine the deuterium uptake at peptide level so as to dissect the interaction interface of PC4 and *trans*-PtTz-platinated dsODN, an online pepsin digestion column was constructed according to a previously reported procedure³⁰ and applied into the HPLC system, as depicted in Scheme 1. Pepsin was employed in the digestion of proteins, which tends to cleave at various positions to give small peptides (3 – 30 amino acids) and functions under acidic condition compatible to the pH of the quenching solution after HDX (pH = 2 – 3). Firstly, apo-PC4 was introduced as a model to evaluate the efficiency of the online pepsin digestion column coupled to a HPLC-ESI-MS system. Totally 20 peptides were identified, covering 86.6% of the sequence of PC4 (Table 1 and Figure S3). The identified peptides were assignable with sufficient signal-to-noise ratios within the error of 60 ppm. Peptides Pep1 – Pep7 were mainly located at the two serine-rich loops that belongs to the flexible N-terminal of PC4. The C-terminal peptides Pep8 – Pep13 cover five β -sheet region which is responsible for the binding of PC4 to ODN. Pep14 – Pep20 belong to the only α -helix region which, in combination with Pep13 from the β -sheet region, is important for PC4 dimerization.⁶⁻⁷ Although there was some overlap among the identified peptides, the potential DNA binding domain of PC4 on the β -sheets^{6-7, 40} were successfully recognized, which provides adequate structural information for localizing the interaction regions between PC4 and 1,3-*trans*-PtTz-**III**.

The deuterium uptake of individual peptic peptide of apo-PC4 and holo-PC4 were measured subjected to a 120 min continuous H/D exchange at 293 K and the deuterium uptake ratio was calculated by Equation 1. The time dependent change in deuterium exchange levels and the ESI mass spectra at 1 and 120 min, respectively, of representative peptides, Pep6 (L49 – M63), Pep13 (I85 – Q109) and Pep16 (W110 – D122), derived from apo- and holo-PC4, are shown in Figure 3. The analogous plots of the rest of the peptides are depicted in Figure S4 – S12 in the Supporting Information. The heat map showing the change of deuteration ratio for all the peptides is in Figure 4. These results indicate that over 120 min of H/D exchange, there were no pronounced change in the deuteration ratio of peptic peptides Pep1 – Pep4, Pep9 – Pep11 and Pep19 – Pep20, which derived from the loop (M1 – K41), β 1 – β 2 sheets (F64 – D84) and C-terminal α -helix (I120 – L127), respectively, between apo- and holo-PC4. However, for peptide Pep5 (T42 – S55), Pep6 (L49 – M63) and Pep7 (S52 – D61), upon binding to 1,3-*trans*-PtTz-**III**, their maximum deuterium uptake significantly decreased compared to apo-PC4, suggesting that the interaction with *trans*-PtTz intrastrand crosslinked ODN prevented the HDX of the backbone amide hydrogens in these peptides. Considering that Pep1 – Pep4 (M1 – S46) were almost not affected in the ratio of deuterium uptake due to the platinated ODN binding, the residues R47 to M63 belonging to the flexible serine-rich loop in the N-terminal (Figure S3) must play an important role in the recognition and interaction with 1,3-*trans*-PtTz-**III**. Significant decrease was also observed in the deuteration ratio of peptic peptides, Pep5 – Pep7 and Pep12 – Pep13, which arose from β 3 – β 5-sheets (I85 – L105) of the holo-PC4 compared to those of the apo-PC4 (Figures 3 – 4 and S4 – S9). These revealed that β 3 – β 5-sheet region are involved in the recognition and binding of PC4 to the 1,3-PtTz crosslinked ODN **III**. Peptic peptides Pep15 – Pep17, which cover residues W110 to D122, were derived from the only α -helix

in PC4. Surprisingly, upon binding to 1,3-*trans*-PtTz-III, their maximum deuterium uptake number significantly increased compared to apo-PC4 (Figures 3 – 4 and S10 – S12). These results indicated that the ligation with 1,3-*trans*-PtTz-III did not occur on the dimerization interface of PC4 but partially loosen the PC4 dimer by binding to the adjacent β -sheet region.⁶⁻⁷

Table 1. Identified peptides 1 – 20 of apo-PC4 by online pepsin digestion coupled with HPLC-ESI-MS.

Peptide	Sequence	Observed (<i>m/z</i>)	Calculated (<i>m/z</i>)	Error (ppm)
Pep1	M ₁ PKSKE ₆	360.1911 ²⁺	360.1915 ²⁺	-1.11
Pep2	M ₁ PKSKELVS ₉	509.7826 ²⁺	509.7837 ²⁺	-2.16
Pep3	M ₁ PKSKELVSSSSSGSDSD ₁₈	914.4224 ²⁺	914.4175 ²⁺	5.36
Pep4	P ₃₆ VKKQKTGETS ₄₆	601.8619 ²⁺	601.8438 ²⁺	30.1
Pep5	T ₄₂ GETSRALSSSKQS ₅₅	719.8495 ²⁺	719.8594 ²⁺	-13.8
Pep6	L ₄₉ SSSKQSSSRDDNM ₆₃	814.8641 ²⁺	814.8594 ²⁺	5.77
Pep7	S ₅₂ KQSSSRDD ₆₁	548.7311 ²⁺	548.7500 ²⁺	-34.4
Pep8	R ₅₉ DDNMFQIGKMRYVSVRDFK ₇₉	854.7437 ³⁺	854.7578 ³⁺	-16.5
Pep9	F ₆₄ QIGKMRY ₇₁	521.7778 ²⁺	521.7813 ²⁺	-6.71
Pep10	I ₆₆ GKMRYV ₇₂	433.7264 ²⁺	433.7495 ²⁺	-53.3
Pep11	R ₇₀ YVSVRDFK GKVLID ₈₄	559.0115 ³⁺	559.0116 ³⁺	-0.18
Pep12	K ₈₀ VLIDIREYWMDPEGE ₉₅	996.9883 ²⁺	996.9904 ²⁺	-2.11
Pep13	I ₈₅ REYWMDPEGEMKPGRKGISLNPEQ ₁₀₉	987.4794 ³⁺	987.4844 ³⁺	-5.06
Pep14	N ₁₀₆ PEQWSQLKEQISDIDD ₁₂₂	1022.9307 ²⁺	1022.9766 ²⁺	-44.9
Pep15	W ₁₁₀ SQL ₁₁₃	553.2738 ⁺	553.2734 ⁺	0.72
Pep16	W ₁₁₀ SQLKEQISDIDD ₁₂₂	788.8779 ²⁺	788.8750 ²⁺	3.68
Pep17	Q ₁₁₂ LKEQISDIDDAVR ₁₂₅	815.4430 ²⁺	815.4297 ²⁺	16.3
Pep18	K ₁₁₄ EQISDIDD ₁₂₂	1062.4957 ⁺	1062.4922 ⁺	3.48
Pep19	I ₁₂₀ DDAVRKL ₁₂₇	465.2752 ²⁺	465.2734 ²⁺	3.87
Pep20	V ₁₂₄ RKL ₁₂₇	515.3652 ⁺	515.3664 ⁺	-2.33



Scheme 1. Schematic set up of the online digestion and peptide separation device in this work. Green arrows indicate the direction of samples and mobile phases. Valve A is in position “inject” (solid lines) and can be switched to “load” (dashed lines). Valve B is in position displayed in solid lines for sample loading in trap column and can be shifted to position in dashed lines for HPLC analysis.

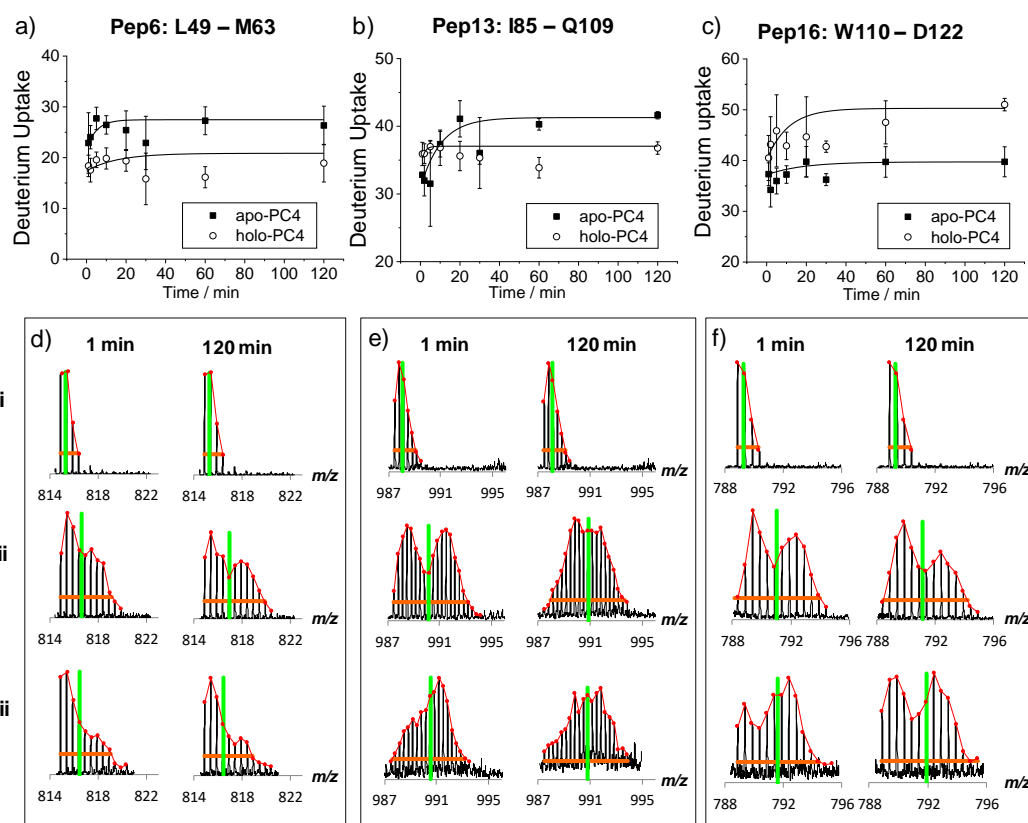


Figure 3. Kinetic curves of H/D exchange of peptic peptides (a) Pep6 (L49 – M63), (b) Pep13 (I85 – Q109) and (c) Pep16 (W110 – D122) arising from apo-PC4 (square) and holo-PC4 (circle). (d, e, f) Mass spectra of non-deuterated (i) and deuterated (ii, iii) peptides for apo-PC4 (ii) and holo-PC4 (iii) incubated in D₂O buffer for 1 min and 120 min, respectively. The vertical green line suggests the centroid *m/z* of each deuterated peptide.

Molecular dynamics simulations

Molecular dynamics simulations were performed to study the interaction details between PC4 and 1,3-*trans*-PtTz-**III**. To do so, we firstly constructed the molecular model of *trans*-PtTz (Figure S13) binding to the double-stranded ODN **III**. Molecular dynamics simulations were then carried out to give the equilibrium structures of 1,3-*trans*-PtTz-**III** complex. The structure in which *trans*-PtTz binds to **III** with its ammonia ligand towards the major groove of duplex **III** was found to be more stable with π - π stacking forming between the five-membered ring of *trans*-PtTz and two guanine residues G6 and G8 (Figure S14) than another in which *trans*-PtTz binds to **III** with its ammonia ligand towards the minor groove of duplex **III** (data not shown). Therefore, this conformation was adopted as the initial structure for dynamics simulation of holo-PC4 complex.

The previous reports showed that the structured C-terminal domain of PC4 usually dimerize to accommodate a single-stranded DNA while the unstructured N-terminal loop was usually neglected for research on PC4-DNA interaction, perhaps due to difficulty in crystallization. As a consequence, no full 3D structure of apo-PC4 is available in PDB. Considering the interaction between the loop and the platinated ODN **III** as revealed by our HDX-MS analysis, we manually added the N-terminal loop (M1 – N62) to the X-ray structure of the DNA binding domain (M63 – L127) deposited in PDB with a code of 2C62⁷ to obtain the equilibrium structure of holo-PC4 ligated with 1,3-*trans*-PtTz-**III** via 2 ns

molecular dynamic simulation. As our global HDX MS results showed that the binding stoichiometry of PC4 to 1,3-*trans*-PtTz-**III** was 1:1, we only simulated the binding of one 1,3-*trans*-PtTz-**III** molecule to one PC4 monomer molecule instead of dimer molecule. PC4-DNA binding can undergo in two ways, i.e. minor groove binding and major groove binding. Thus, we docked the generated apo-PC4 model into the major and minor groove of 1,3-*trans*-PtTz-**III** complex, respectively, for energy minimization (Figures S15). The results showed that the root mean square deviation (RMSD) value of the minor groove binding complex became stable in only 2 ns stimulation (Figure S15A) and that the minor groove binding produced much lower potential energy than the major groove binding (Figure S15B). This suggests that PC4 preferentially binds to the minor groove of 1,3-*trans*-PtTz-**III** (Figure 5 and Figure S16).

Further analysis indicated that in the model of minor groove binding complex, two regions of PC4, T42 – D61 of the serine-rich loop and M63 – Q109 at the β -sheets, have relatively strong interactions with the minor groove of 1,3-*trans*-PtTz-**III** complex (Figure 5), which is well consistent with HDX-MS results described above. The hydrogen bonds and Van der Waals interactions between the β -sheet region of PC4 and 1,3-*trans*-PtTz-**III** made the minor groove width twice as much as those in intact dsODN **III** over bases T5 to T7 (insert in Figure 5, see also Figure S17 for comparison with those of the major groove binding holo-PC4). These suggests that the 1,3-*trans*-PtTz crosslinking partially unwound the duplex **III** into a conformation in a certain manner of single strands, favoring the binding of PC4, which is supported by the special single-stranded DNA binding capacity of PC4.^{7, 14, 21} As a consequence, the minor groove width was in turn further broadened at T5 to T7 and narrowed at G8 to T10, leading to strong protein-DNA interaction at this region.

In order to further evaluate the interactions at the interface of PC4 with 1,3-*trans*-PtTz-**III**, in particular at the β -sheets and the loop region, hydrogen bond occupancy and H-O distances which indicates the stability and the strength of hydrogen bonds were analysed, respectively. As shown in Table 2, the side chains of Arg86 and Arg100 in the β 3- and β 5-sheets, respectively, of PC4 form stable hydrogen bonds with C25 and A24 residues of the complementary strand **II** opposite to the platination site of ODN **III**. The hydrogen bond between OP1@C25 and HH22@Arg86 is the most stable one and the occupancy reaches 69.38%. Meanwhile, OP1@C25 forms another strong hydrogen bond with HE12@Arg86. These two bonds can be very stable except a short period in the simulations, as shown in Figure S18. OP2@A24 in ODN **III** forms two hydrogen bonds with HE and HH21@Arg100 in PC4. These four H-bonds have 50 – 70% occupancy, and exist in pair to enhance the stability of connection between PC4 and 1,3-*trans*-PtTz-**III**. At the serine-rich loop region of PC4, three relatively stable hydrogen bonds, HH12 and HH22@Arg59 with OP1@T10, and HH12@Arg47 with OP2@G17, respectively, can be observed. These H-bonds have lower (10 – 15%) occupancy and the bond lengths are around 2.81 Å.

The occupancy of H-bonds formed in the interface of PC4 binding to the major groove of 1,3-*trans*-PtTz-**III** is much lower, compared with those in the minor groove binding complex. This again verifies that PC4 prefers to bind to the minor groove of 1,3-*trans*-PtTz-**III**, remarkably contributed to the H-bonds between Arg86, Arg100 residues in β 3 - β 5 sheets of PC4 and A24, C25 residues of 1,3-*trans*-PtTz-**III**. The serine-rich loop may also play some roles in the interaction, perhaps *via* forming H-bonds with T10 and G17 in the platinated ODN **III**.

Electrophoretic mobility shift assays (EMSAs)

EMSAs were performed to provide an additional support to binding sites at single amino acid residue level for the interaction of PC4 with the platinated ODN **III**. Fluorescein-labeled single-stranded **II** (F-**II**) was used to produce fluorescent 1,3-*trans*-PtTz-**III** complex. EMSAs were respectively run for

platinated **III** complex, intact ODN **III** and three types of PC4 proteins, i.e. wild-type PC4, site-directed mutants PC4(R86A) and PC4(S104P). As shown in Figure 6a and d, when the molar ratio of the wild type PC4 versus 1,3-*trans*-PtTz-**III** was raised to 8:1 or above, the lagging bands of the platinated ODN were observed. For comparison, for the non-platinated **III** the lagging band did not occur until the molar ratio reached 12:1. This indicates that PC4 binds to 1,3-*trans*-PtTz-**III** stronger than to non-platinated **III**.

In the presence of PC4(R86A) mutant, lagging band was not observed for 1,3-*trans*-PtTz-**III** until the molar ratio of protein to ODN reached 128:1 (Figure 6b). Whereas pronounced lagging band of the intact ODN **III** arose when the molar ratio of PC4(R86A) mutant versus **III** was higher than 48:1. This suggests that the mutation at Arg86 significantly impeded the interaction of PC4 with the platinated ODN, but less impacted on the interaction between PC4 and native double-stranded ODN. In other words, the Arg86 residue plays a crucial role in the recognition and interaction of PC4 with 1,3-*trans*-PtTz-**III**. When Ser104 of PC4 was mutated to proline, the lagging band for both the platinated and non-platinated **III** appeared when the molar ratio of PC4(S104P) versus 1,3-*trans*-PtTz-**III** or intact **III** was higher than 24:1 (Figure 6c, f), indicating that the S104P mutation also reduced the binding affinity of PC4 with ODN, but did not discriminate 1,3-*trans*-PtTz crosslinked **III** and intact **III**.

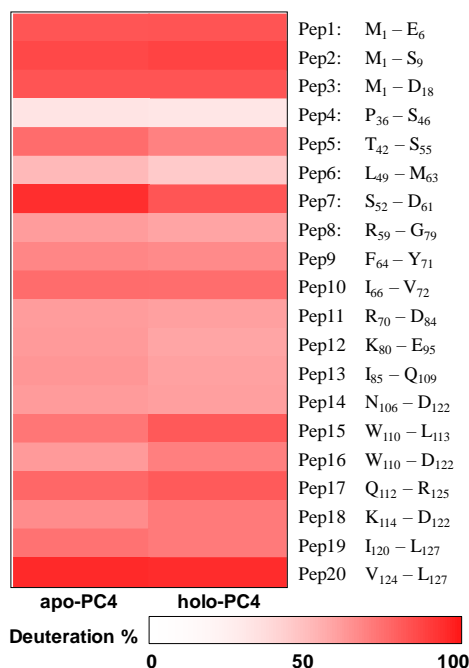


Figure 4. Heat map for deuterium ratio of amides in peptic peptides arising from apo- and holo-PC4 as assessed by HDX-MS. The relative deuterium rates were measured after 120 min of incubation of the proteins in D₂O buffer, and are assigned according to the color bar shown in the bottom. Also see the location of each peptide in the protein in Figure S3.

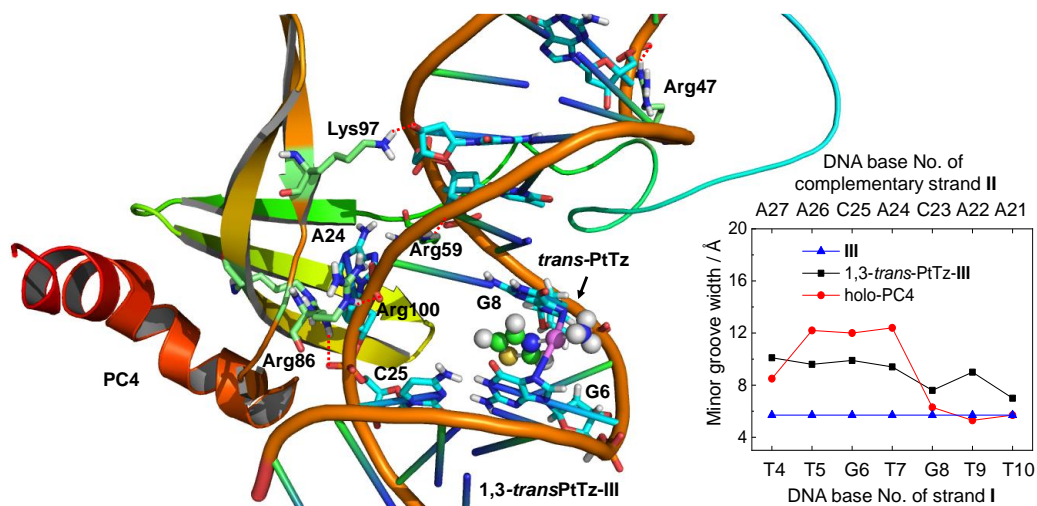


Figure 5. The simulated conformation of PC4 binding at the minor groove of 1,3-*trans*-PtTz-III complex. Hydrogen bonds are shown in red dotted lines. It is notable that Arg86 and Arg100 form H-bonds with C25 and A24, respectively, of the complementary strand opposite to the platination site. The insert shows the minor groove width of intact dsODN III, 1,3-*trans*-PtTz-III and holo-PC4 complex.

Table 2. Hydrogen bond formation, occupancy and confirmation of holo-PC4 (minor groove).

Acceptor atom @ODN base	Donor atom @amino acid	Occupancy (%)	Average Distance (Å)	Average Angle (°)
OP1@C25	HH22@Arg86	69.38	2.825	152.6
OP2@A24	HE@Arg100	68.61	2.828	152.6
OP2@A24	HH21@Arg100	61.99	2.807	150.2
OP1@C25	HH12@Arg86	53.79	2.831	150.8
OP1@T10	HH12@Arg59	14.69	2.814	155.3
OP1@T10	HH22@Arg59	13.46	2.810	154.8
OP1@C11	HZ2@Lys97	12.82	2.818	152.3
OP2@G17	HH12@Arg47	12.52	2.804	156.1
OP1@C11	HZ3@Lys97	10.41	2.814	152.7

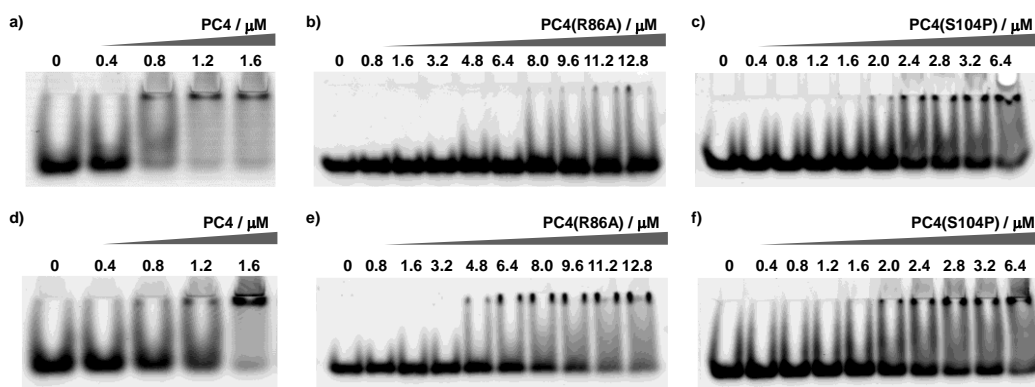


Figure 6. Electrophoretic mobility shift assays (EMSA) of double-stranded ODN duplex in the presence of various type of PC4 proteins. (a – c) 1, 3-*trans*-PtTz-**III** (0.1 μ M) and (d – f) duplex **III** (0.1 μ M) incubated with various concentration of wild type PC4 (a, d), PC4(R86A) mutant (b, e) and PC4(S104P) mutant (c, f).

Discussion

The human positive cofactor 4 (PC4) contains two major domains: the DNA-binding C-terminal domain (M63 –L127) and the flexible serine- or lysine-rich regulatory domain at the N-terminal (M1 – N62).¹¹⁻¹² The conserved C-terminal, consisting of a curved five pieces of anti-parallel β -sheets followed by a 45° kinked α -helix, is essential for its functions in binding to ssDNA and therefore transduct the repair signal of DNA damage and prevent genome instability.^{4, 13, 21, 41}

In previous reports, the crystal structure of PC4 showed that the C-terminal domain tends to form homodimers, in which two ssDNA binding channels can be formed in opposite direction.^{6-7, 42} The kinked α -helix, packing against the β -sheets of their respective dimeric partner, forms the central hydrophobic core, favoring the binding of ssDNA as well as the unwound complementary strands or mismatch heteroduplex DNA. In this work, in order to simplify computational procedure, we adopted the conformation of PC4 monomer from the crystal structure of the homodimer to perform the molecular dynamic simulation. As the binding stoichiometry of PC4 to 1,3-*trans*-PtTz-**III** was measured to be 1:1, using one of each molecule in the simulation can produce adequate information. Furthermore, we obtained the equilibrated conformation of the full 1,3-*trans*-PtTz-**III**-PC4 complex, where the platinated ODN duplex partially unwind due to *trans*-PtTz binding, making it suitable to be specially recognized by PC4. The K80 – Q109 residues at β 3, β 4 and β 5-sheet region of PC4 comprises DNA binding interfaces. Among these amino acid residues, the positively charged side chains such as Arg86 and Arg100 form strong H-bonds with the negatively charged phosphate backbone of C25 and A24 in the ODN strand **II**, and play key roles in the recognition of PC4 with the 1,3-*trans*-PtTz crosslinked ODN duplex. This result is in consistence with a previous report that mutation of Arg86 substantially reduced the affinity with ssDNA.^{40, 42} On the other hand, this finding also evidences that the 1,3-*trans*-PtTz crosslinking damaged double stranded ODN was unwound to behave in the manner of single strand, which favour the recognition and binding of PC4. Given that PC4 is an early responding protein to DNA damage, the recognition of the transplatin-induced lesions on DNA may initiate DNA repair, which in turn recovers DNA replication and transcription and diminishes cytotoxicity of this transplatin complex. Indeed, most recently we discovered that downregulating the expression of PC4 could promote the cytotoxicity of *trans*-PtTz. The results will be published elsewhere.

The N-terminal of PC4 are serine- or lysine-rich domain. Although highly flexible and unstructured, it can still play regulatory role for the interaction activity of the structured C-terminal core domain through modulation and/or shielding of the interaction surface.⁴⁰ In this work, the moderate interaction of serine-rich region (R47 – M63) was also revealed by both HDX-MS analysis and molecular dynamics simulation, showing that the flexible domain can also be involved in the unique interaction of PC4 with the 1,3-*trans*-PtTz crosslinked ODN. The arginine residues (Arg47 and Arg59) also form H-bonds with the phosphate backbone of ODN.

In the present work, HDX MS data and molecular simulation constructed a network of electrostatic and hydrophobic interactions between PC4 and 1,3-*trans*-PtTz crosslinked dsODN. This is the first report, to our best knowledge, to describe the structure basis of the interaction between PC4 and a platinum complex damaged double-stranded ODN. More importantly, we discovered that the usually overlooked flexible loop region of PC4 also played a regulatory role for the interaction of PC4 with 1,3-*trans*-PtTz damaged dsODN in addition to the highly structured β -sheets. Moreover, our HDX-MS results indicated that 1,3-*trans*-PtTz-III binding to PC4 appeared to partially loosen the interface of PC4 dimer. Whether and how this action impacts PC4 biological functions as a transcription cofactor warrants further investigation.

Conclusions

In summary, hydrogen/deuterium exchange mass spectrometry (HDX-MS) combined with online pepsin digestion and molecular dynamics simulations has been applied herein to study the unique recognition and interaction of PC4 protein with 1,3-GTG intrastrand crosslinked dsODN by *trans*-PtTz complex. The kinetic results of global deuterium uptake, showing a significant decrease of exchangeable backbone amide hydrogens of PC4 after binding to 1,3-*trans*-PtTz crosslinked dsODN, confirmed their specific interactions. Further local deuterium uptake kinetics study indicated that R47 – M63 at the serine-rich loop region and K80 – Q109 at the β -sheet region of PC4 were mainly involved in the interactions with the *trans*-platinum complex crosslinked dsODN. Molecular dynamics simulations revealed that Arg86 and Arg100 formed stable H-bonds with ODN backbone phosphate group, and played a crucial role in the unique interaction. The Arg86 residue of PC4 was further verified by EMSA as a key amino acid residue for the specific recognition between 1,3-*trans*-PtTz-III and PC4. More significantly, the structural basis for the interaction of PC4 with *trans*-platinum damaged DNA provided novel insights to elucidate the regulation effect of PC4 to the repair of *trans*-PtTz damaged DNA, so as to predict the influence to the anticancer activity of this platinum complex. The successful application of the method by combining HDX-MS with online pepsin digestions and molecular dynamics simulations can be further widely spread to study the interactions between other intact or/and damaged DNA and proteins.

ASSOCIATED CONTENT

Supporting Information

The Supporting Information is available free of charge on the ACS Publications website. To allow access to the HDX data of this study, the HDX data summary table (Supporting data table 1) and the HDX data tables (Supporting data table 2 and 3) are also included as per consensus guidelines of HDX MS.⁴³

AUTHOR INFORMATION

Author Contributions

F.W. and Y.Z. conceived and designed the project. F.W., Y.Z. and X.Z. supervised the project. Y.W., Z.D., K.W. and Q.L. performed the HDX-MS and EMSA experiments, L.C., W.Z. and H.Z. performed the molecular simulations. Y.W., J.Q. and L.Q. fabricated the online pepsin digestion column. Y.W., Z.D., F.W., X.Z. and Y.Z. analysed data, wrote and revised the manuscript. All authors have given approval to the final version of the manuscript.

Conflicts of interest

The authors declare no competing financial interest.

ACKNOWLEDGMENT

We thank Professor Yangzhong Liu of University of Science and Technology of China for providing the *trans*-PtTz complex as a gift. We thank the National Natural Science Foundation of China (grant nos. 21927804, 21635008, 21575145) and the Youth Innovation Promotion Association of Chinese Academy of Sciences (grant no. 2017051) for support.

REFERENCES

1. M. Garavís and O. Calvo, *Cur. Gen.*, 2017, **63**, 1023-1035.
2. A. Tavenet, A. Suleau, G. Dubreuil, R. Ferrari, C. Ducrot, M. Michaut, J.-C. Aude, G. Dieci, O. Lefebvre, C. Conesa and J. Acker, *Proc. Natl. Acad. Sci. USA*, 2009, **106**, 14265-14270.
3. Z. Q. Pan, H. Ge, A. A. Amin and J. Hurwitz, *J. Biol. Chem.*, 1996, **271**, 22111-22116.
4. J. Y. Wang, A. H. Sarker, P. K. Cooper and M. R. Volker, *Mol. Cell. Bio.*, 2004, **24**, 6084-6093.
5. H. Ge and R. G. Roeder, *Cell*, 1994, **78**, 513-523.
6. J. Brandsen, S. Werten, P. C. van der Vliet, M. Meisterernst, J. Kroon and P. Gros, *Nat. Struct. Biol.*, 1997, **4**, 900-903.
7. S. Werten and D. Moras, *Nat. Struct. Mol. Biol.*, 2006, **13**, 181-182.
8. M. Hyjek-Składanowska, T. A. Vickers, A. Napiórkowska, B. A. Anderson, M. Tanowitz, S. T. Crooke, X.-h. Liang, P. P. Seth and M. Nowotny, *J. Am. Chem. Soc.*, 2020, **142**, 7456-7468.
9. S. Werten, G. Stelzer, A. Goppelt, F. N. Langen, P. Gros, H. T. M. Timmers, P. C. Van der Vliet and M. Meisterernst, *EMBO J.*, 1998, **17**, 5103-5111.
10. D. Wang and S. J. Lippard, *Nat. Rev. Drug Discov.*, 2005, **4**, 307-320.
11. S. Werten, F. W. M. Langen, R. van Schaik, H. T. M. Timmers, M. Meisterernst and P. C. van der Vliet, *J. Mol. Biol.*, 1998, **276**, 367-377.
12. K. Kaiser, G. Stelzer and M. Meisterernst, *EMBO J.*, 1995, **14**, 3520-3527.
13. K. Batta, M. Yokokawa, K. Takeyasu and T. K. Kundu, *J. Mol. Biol.*, 2009, **385**, 788-799.
14. O. Mortusewicz, W. Roth, N. Li, M. C. Cardoso, M. Meisterernst and H. Leonhardt, *J. Cell Biol.*, 2008, **183**, 769-776.
15. E. R. Jamieson and S. J. Lippard, *Chem. Rev.*, 1999, **99**, 2467-2498.
16. Y. W. Jung and S. J. Lippard, *Chem. Rev.*, 2007, **107**, 1387-1407.
17. J. M. Perez, M. A. Fuertes, C. Alonso and C. Navarro-Ranninger, *Crit. Rev. Onco. Hemat.*, 2000, **35**, 109-120.
18. T. Suchankova, M. Vojtiskova, J. Reedijk, V. Brabec and J. Kasparkova, *J. Biol. Inorg. Chem.*, 2009, **14**, 75-87.
19. V. Marini, P. Christofis, O. Novakova, J. Kasparkova, N. Farrell and V. Brabec, *Nucleic Acids Res.*, 2005, **33**, 5819-5828.

20. Z. Du, Q. Luo, L. Yang, T. Bing, X. Li, W. Guo, K. Wu, Y. Zhao, S. Xiong, D. Shangguan and F. Wang, *J. Am. Chem. Soc.*, 2014, **136**, 2948-2951.
21. O. Mortusewicz, B. Evers and T. Helleday, *Oncogene*, 2016, **35**, 761-770.
22. M. J. Chalmers, S. A. Busby, B. D. Pascal, G. M. West and P. R. Griffin, *Exp. Rev. Proteomics*, 2011, **8**, 43-59.
23. D. P. Marciano, V. Dharmarajan and P. R. Griffin, *Curr. Opin. Struct. Biol.*, 2014, **28**, 105-111.
24. K. D. Rand, M. Zehl and T. J. D. Jorgensen, *Acc. Chem. Res.*, 2014, **47**, 3018-3027.
25. L. Huang, P.-K. So, Y. W. Chen, Y.-C. Leung and Z.-P. Yao, *J. Am. Chem. Soc.*, 2020, **142**, 13756-13767.
26. J. E. Longbotham, C. M. Chio, V. Dharmarajan, M. J. Trnka, I. O. Torres, D. Goswami, K. Ruiz, A. L. Burlingame, P. R. Griffin and D. G. Fujimori, *Nat. Commun.*, 2019, **10**.
27. E. Trabjerg, N. Abu-Asad, Z. Wan, F. Kartberg, S. Christensen and K. D. Rand, *Structure*, 2019, **27**, 1103-1113.e1103.
28. X. Ye, J. B. Lin, L. Mayne, J. Shorter and S. W. Englander, *Proc. Natl. Acad. Sci. USA*, 2019, **116**, 7333-7342.
29. M. Vanbeusichem and N. Farrell, *Inorg. Chem.*, 1992, **31**, 634-639.
30. C. Yao, L. Qi, W. Hu, F. Wang and G. Yang, *Anal. Chim. Acta*, 2011, **692**, 131-137.
31. T. Jiang, J. Jiskra, H. A. Claessens and C. A. Cramers, *J. Chromatogr. A*, 2001, **923**, 215-227.
32. M. Guttman, D. D. Weis, J. R. Engen and K. K. Lee, *J. Am. Soc. Mass. Spectrom.*, 2013, **24**, 1906-1912.
33. R. E. Duke, T. J. Giese, H. Gohlke, A. W. Goetz, N. Homeyer, S. Izadi and LeGrand Amber 14, University of California: San Francisco, CA, USA, 2015.
34. J. D. Chai and M. Head-Gordon, *Phys. Chem. Chem. Phys.*, 2008, **10**, 6615-6620.
35. M. J. Fisch, G. W. Trucks, H. B. Schlegel, G. E. Scuseria, M. A. Robb, J. R. Cheeseman, G. Scalmani, V. Barone, B. ennucci and G. A. Petersson *Gaussian 09 Revision D. 01.*, Gaussian: Wallingford, CT, USA, 2009.
36. S. Zheng, Q. Tang, J. He, S. Du, S. Xu, C. Wang, Y. Xu and F. Lin, *J. Chem. Inf. Modeling*, 2016, **56**, 811-818.
37. R. Lavery, M. Moakher, J. H. Maddocks, D. Petkeviciute and K. Zakrzewska, *Nucleic Acids Res.*, 2009, **37**, 5917-5929.
38. J. Wang, R. M. Wolf, J. W. Caldwell, P. A. Kollman and D. A. Case, *J. Comput. Chem.*, 2004, **25**, 1157-1174.
39. A. Poliakov, P. Jardine and P. E. Prevelige, *Rapid Commun. Mass Spectrom.*, 2008, **22**, 2423-2428.
40. H. R. A. Jonker, R. W. Wechselberger, R. Boelens, R. Kaptein and G. E. Folkers, *Biochemistry*, 2006, **45**, 5067-5081.
41. R. B. Caldwell, H. Braselmann, U. Schoetz, S. Heuer, H. Scherthan and H. Zitzelsberger, *Sci. Rep.*, 2016, **6**.
42. S. Werten, R. Wechselberger, R. Boelens, P. C. van der Vliet and R. Kaptein, *J. Biol. Chem.*, 1999, **274**, 3693-3699.
43. G. R. Masson, J. E. Burke, N. G. Ahn, G. S. Anand, C. Borchers, S. Brier, G. M. Bou-Assaf, J. R. Engen, S. W. Englander, J. Faber, R. Garlish, P. R. Griffin, M. L. Gross, M. Guttman, Y. Hamuro, A. J. R. Heck, D. Houde, R. E. Iacob, T. J. D. Jorgensen, I. A. Kaltashov, J. P. Klinman, L. Konermann, P. Man, L. Mayne, B. D. Pascal, D. Reichmann, M. Skehel, J. Snijder, T. S. Strutzenberg, E. S. Underbakke, C. Wagner, T. E. Wales, B. T. Walters, D. D. Weis, D. J. Wilson, P. L. Wintrode, Z. Q. Zhang, J. Zheng, D. C. Schriemer and K. D. Rand, *Nat. Met.*, 2019, **16**, 595-602.

Table of Contents

Structural basis of human nuclear protein positive cofactor PC4 binding to a platinum damaged double-stranded DNA is revealed by hydrogen exchange mass spectrometry combined with molecular dynamics simulation.

